The New Putative Type III Effector SkP48 in Bradyrhizobium sp. DOA9 is Involved in Legume Nodulation

Pongdet Piromyou
Suranaree University of Technology
Pongpan Songwattana
Suranaree University of Technology
Pakpoom Boonchuen
Suranaree University of Technology
Hien P. Nguyen
Tokyo University of 18 Agriculture and Technology (TUAT)
Monchai Manassila
Soil Microbiology Research Sub-Group, Soil Science Research Group, Agricultural Production Science Research and Development Division, Department of Agriculture
Waraporn Tantanuch
Synchrotron Light Research Institute
Bussayarat Maikhunthod
Synchrotron Light Research Institute
Kamonluck Teamtisong
The Center for Scientific and Technological Equipment, Suranaree University of Technology
Panlada Tittabut
Suranaree University of Technology
Nantakorn Boonkerd
Suranaree University of Technology
Eric Giraud
IRD, Laboratoire des Symbioses Tropicales et Méditerranéennes, UMR 113, IRD/CIRAD/INRAE/Université de Montpellier/SupAgro. Campus de Baillarguet, TA-A82/J, 34398 Montpellier Cedex 5
Neung Teaumroong (neung@sut.ac.th)
Suranaree University of Technology

Research Article

Keywords: T3SS, SkP48, symbiosis, Bradyrhizobium sp. DOA9, Vigna radiata

Posted Date: September 27th, 2021

DOI: https://doi.org/10.21203/rs.3.rs-900464/v1

The New Putative Type III Effector SkP48 in *Bradyrhizobium* sp. DOA9 is Involved in Legume Nodulation

Authors: Pongdet Piromyou[1†]

Pongpan Songwattana[1†]

Pakpoom Boonchuen[1]

Hien P. Nguyen[2]

Monchai Manassila[3]

Waraporn Tantanuch[4]

Bussayarat Maikhunthod[4]

Kamonluck Teamtisong[5]

Panlada Tittabut[1]

Nantakorn Boonkerd[1]

Eric Giraud[6*]

Neung Teaumroong[1*]

Address: 1 School of Biotechnology, Institute of Agricultural Technology, Suranaree University of Technology, Nakhon Ratchasima 30000, Thailand

2 Institute of Global Innovation Research (IGIR), Tokyo University of Agriculture and Technology (TUAT), Fuchu, Tokyo 183-8538, Japan

3 Soil Microbiology Research Sub-Group, Soil Science Research Group, Agricultural Production Science Research and Development Division, Department of Agriculture, Bangkok 10900, Thailand

4 Synchrotron Light Research Institute, University Avenue, Muang District, Nakhon Ratchasima 30000, Thailand

5 The Center for Scientific and Technological Equipment, Suranaree University of Technology, Nakhon Ratchasima 30000, Thailand

6 IRD, Laboratoire des Symbioses Tropicales et Méditerranéennes, UMR 113, IRD/CIRAD/INRAE/Université de Montpellier/SupAgro. Campus de Baillarguet, TA-A82/J, 34398 Montpellier Cedex 5, France

† These authors contributed equally as co-first authors: Pongdet Piromyou and Pongpan Songwattana

*Correspondence:

Eric Giraud

eric.giraud@ird.fr

Neung Teaumroong

Tel: +66-44-223-389; Fax: +66-44-216-345

neung@sut.ac.th

Abstract. *Bradyrhizobium* sp. DOA9 can nodulate a wide spectrum of legumes; however, unlike other bradyrhizobia, DOA9 carries a symbiotic plasmid harboring type III secretion system (T3SS) and several effector (T3E) genes, one of which encodes a new putative type III effector—SkP48. Here, we demonstrated the pivotal roles of SkP48 from *Bradyrhizobium* sp. DOA9 in inhibiting nodulation of various *Vigna* species and *Crotalaria juncea* and suppressing

nodulation efficiency of *Arachis hypogea*. By contrast, the nodulation efficiency of a SkP48 mutant did not differ significantly with the DOA9 wild-type strain on *Macroptilium atropurpureum* and *Stylosanthes hamata*. An evolutionary analysis revealed that the SkP48 effector which contains a shikimate kinase and a SUMO protease (C48 cysteine peptidase) domain is distinct from the others effectors previously identified in others bradyrhizobia and pathogenic bacteria. Our findings suggest that the new putative T3E SkP48 is a key factor suppressing nodulation and nodule organogenesis in several legumes by activation of effector-triggered immunity through salicylic acid biosynthesis induction, which is deleterious to rhizobial infection. In addition, nodulation may be modulated by the function of defensins involved in jasmonic acid signalling in *V. radiata* SUT1.

Keywords: T3SS, SkP48, symbiosis, *Bradyrhizobium* sp. DOA9, *Vigna radiata*

Introduction. Symbiotic nitrogen fixation culminates in a series of complex chemical interactions between leguminous plants and their compatible rhizobia through specific recognition of the two partners involved. Typically, symbiosis is initiated in N-limited soils, where flavonoids secreted by legumes are recognized as signal molecules by rhizobia, which secret in return Nod factors (NFs). Subsequently, the perception of NFs by plant receptors triggers a series of plant responses, nodule organogenesis and bacterial infection processes [1,2]. In addition to NFs, other bacterial components, including exopolysaccharides (EPS), lipopolysaccharides (LPS), capsular polysaccharides (KPS), and cyclic β-glucans, are important for rhizobium–legume symbiosis [3,4]. Furthermore, in several strains of *Bradyrhizobium*, *Rhizobium* and *Sinorhizobium*, the type III secretion system (T3SS) is also activated by flavonoids [5–9]. The T3SS of rhizobia shares homology with the T3SS apparatus of plant and animal pathogenic bacteria and permits the delivery of type III effectors (T3E) into

68 the cytosol of eukaryotic host cells [5]. Some secreted T3Es play positive roles in nodulation by
69 suppressing plant immunity, thereby facilitating bacterial infection [10–13]. Conversely, some
70 T3Es are recognized by plant resistance (R) proteins, leading to the activation of effector-
71 triggered plant defence and consequent inhibition of nodulation and nodule organogenesis [7,9].

72 The *Bradyrhizobium* sp. DOA9 strain can induce the formation of nodules in a large spectrum
73 of legume hosts [14]. Interestingly, this strain possesses a symbiotic plasmid harboring *nod, nif*
74 and T3SS genes [15]. While DOA9 T3SS inhibits nodulation in *Vigna radiata*, *Crotalaria juncea*,
75 *Arachis hypogea*, and *Macroptilium atropurpureum*, it positively regulates symbiosis with
76 *Stylosanthes hamata* [16]. Genome mining analysis based on combined searches for homologies
77 to known T3Es and/or the presence in the promoter regions of a regulatory *tts* box, i.e. the DNA
78 motif on which the activator TtsI binds to activate T3SS and T3Es genes expression, has
79 permitted to identify 14 putative T3Es genes in the DOA9 genome [16]. Among them, a new
80 putative T3Es, found on the DOA9 symbiotic plasmid, that we named here SkP48-contains a
81 shikimate kinase and a SUMO protease (C48 cysteine peptidase) domains.

82 Here, we demonstrated that SkP48 from *Bradyrhizobium* sp. DOA9 plays key roles in
83 inhibiting nodulation in various *Vigna* species and *C. juncea* and suppressing nodulation
84 efficiency in *A. hypogea*.

85 ***Results***

86 ***Analysis of the new putative T3E SkP48 and its phylogenetic relationships***

87 The *Bradyrhizobium* sp. DOA9 harbors a T3SS previously shown to modulate positively or
88 negatively the nodulation of several legume species [16,17]. Among the putative T3Es found in
89 the DOA9 genome, a large putative T3E (3,069 amino acids, 335.7 kDa) (Figure 1A) and its
90 *tts*-box were identified on the symbiotic plasmid (gene ID WP_025038828.1) [16]. It shares

homology with some virulence effectors from plant pathogenic bacteria and rhizobia, such as *Xanthomonas oryzae* pv. *oryzae* strain ICMP3125 (30.25% identity), *Pseudomonas savastanoi* pv. *phaseolicola* 1448A (31.39% identity), *Ralstonia solanacearum* GMI1000 (31.62% identity), and *Mesorhizobium loti* MAFF303099 (59.86% identity) (Figure 1B). The amino acid sequence at the carboxyl terminus (2,535 to 2,691) of this T3E displays a shikimate kinase (SK) (EC 2.7.1.71) domain. Phylogenetic analysis based on the amino acid sequence of SK domains identified in putative T3Es of rhizobia and plant pathogens showed that rhizobial T3Es harboring SK domain form 3 distinct clusters: i) cluster 1 grouping T3Es from various *Bradyrhizobium* and *Mesorhizobium* strains, ii) cluster 2 grouping T3Es from *Ensifer* and *Sinorhizobium* species and *Rhizobium etli*, and iii) cluster 3 which groups only WP_025038828.1 and a putative effector identified in *B. elkanii* NBRC14791 (Figure S1B).

Moreover, a small ubiquitin-like modifier (SUMO) protease domain of the C48 peptidase [ubiquitin-like protease 1 (Ulp1)] family is present at amino acids 2,778 to 2,958 of WP_025038828.1 (Figure 1A and S1A). ULP1, a cysteine protease, was first identified in yeast (*Saccharomyces cerevisiae*). It is responsible for eukaryotic protein de-ubiquitination and essential for cell cycle progression [18]. The Ulp1 domain identified in WP_025038828.1 shares similarity with some virulence effectors from pathogenic bacteria, such as XopP of *Xanthomonas campestris* pv. *vesicatoria* strain 85–10 (35% identity), as well as with effector proteins from symbiotic bacteria, such as BEL2-5 of *B. elkanii* (55.08 % of identity; Figure 1B) [13]. To our knowledge, it is the first time that it is reported an effector protein harboring at the same time a SK and a Ulp1 protein domain, suggesting that WP_025038828.1 corresponds to a new putative type of effector that we name shikimate kinase-SUMO peptidase C48 (SkP48)-containing effector.

To determine whether *SkP48* expression is under the control of plant-derived flavonoids, *SkP48* expression in DOA9 and a T3SS-lacking DOA9 mutant (Ω*rhcN*) was determined in presence

and absence of the genistein flavonoid, previously shown to induce T3SS genes and T3Es in several rhizobia [6,17]. As shown in Figure 1C, genistein strongly induced *SkP48* expression in DOA9 cells (2 – 3 times) and moderately in the Ω*rhcN* mutant strain. Therefore, *SkP48* in DOA9 is classically activated by flavonoids, most probably through a T3SS regulatory circuit involving the transcriptional activator TtsI.

Role of SkP48 in legume symbiosis

The DOA9 T3SS negatively affects symbiosis with *V. radiata*, *C. juncea*, *A. hypogea*, and *M. atropurpureum* [16,17]. To further explore the roles of the putative T3E SkP48 in nodulation, full-length of *SkP48* (9,210 bp) was completely deleted to obtain the Δ*SkP48* mutant. Interestingly, at 10 dpi, Δ*SkP48* inoculation significantly induced nodules formation in *V. radiata* (mung bean) cv. SUT1 (SUT1), similar to injectisome mutant (Ω*rhcN*) inoculation, but DOA9 wild-type (WT) inoculation did not (Figure 2 and Table S1). At 15 and 30 dpi the effect of the *SkP48* and *RhcN* mutations remained drastic, DOA9 WT inoculation induced the formation of small necrotic nodules, while Ω*rhcN* and *ΔSkP48* mutant inoculation induced the formation of abundant perfectly developed nodules (Figures 2M). Cytological analyses confirmed that nodules infected by Ω*rhcN* and *ΔSkP48* mutants were normal (Figure 2E, F, H and I) and filled with viable bacteroids (Figure 2K and L), whereas nodules infected by DOA9 WT were necrotic (Figures 2D and 2G), and filled with death bacteria as revealed by red PI staining (Figure 2J). Furthermore, although only a low nitrogenase activity could be detected from 30 dpi in the roots of plants nodulated with the *ΩrhcN* and *ΔSkP48* mutant strains compared with plants inoculated with the DOA9 WT strain, this activity provided a significant benefit on plant growth (Figures 2N and 2O). When, the mutant was tested on different ecotypes of *V. radiata* (13 ecotypes tested), similar observation was done (Table S1). Therefore, SkP48 appears to plays an important role in the induction of symbiotic incompatibility with the *V. radiata* species (Figure 2 and Table S1).

We also analyzed the effect of the S*KP4*8 mutation on another *Vigna species (V. mungo)* which is of agronomic interest. At 30 dpi, we observed that *V. mungo* inoculated with DOA9 WT induced ineffective brownish necrotic nodules (Figure 2P). In contrast, *V. mungo* inoculated with Ω*rhcN* and *ΔSkP48* mutants formed normal symbiotic nodules, with viable bacteroids, as evidenced by green SYTO9 staining (Figure 2T and U). Although it was observed an higher number of nodules on the plants inoculated with DOA9, these ones were clearly not functional as revealed by measurement of the nitrogenase activity and plant dry weight. Perhaps, plants compensated for the ineffective nodules formed by DOA9 WT by increasing nodule number (Figure 2V - X).

In *C. juncea*, at 30 dpi, DOA9 WT only elicited bumps or pseudo-nodules, whereas the *ΩrhcN* and Δ*SkP48* strains formed a high number of perfectly developed and reddish nodules (Figure 3A-J). Similar to the observations in *V. radiata* and *V. mungo,* at 30 dpi, plant dry weight and nitrogen fixation ability of *C. juncea* inoculated with Ω*rhcN* and Δ*SkP48* were significantly higher than those of plants inoculated with DOA9 WT (Figure 3K and L).

In *A. hypogea*, at 30 dpi, nodule formation in plants inoculated with DOA9 WT was significantly lower than that in plants inoculated with Ω*rhcN* and Δ*SkP48* (by ~2.2- and 2-fold, respectively. Although, the nodules derived from DOA9 WT were normal and filled with viable bacteroids as observed for *ΩrhcN*, and Δ*SkP48* mutants (Figure 4A-J), the plants inoculated with the two mutants showed increased nitrogen fixation ability and dry weight compared with those inoculated with DOA9 WT (Figure 4K and L). In contrast, nodulation efficiency of *M. atropurpureum* and *S. hamata* was not significantly different when inoculated with DOA9 WT or its derivative mutants Δ*SkP48* and *ΩrhcN* (Table S1).

Taken together, these results indicate that the negative effects of T3SS previously observed in DOA9 strain are mainly due to the putative T3E SkP48 which after translocation via T3SS should trigger defense responses in some legumes repressing infection and/or nodulation.

SkP48-mediated regulation of plant defence-related genes in legumes

Our previous results showed that the inability of DOA9 strain to nodulate several legume species, including different *Vigna spp.* is due to the putative SK48 T3E. Considering that the genome sequence of *V. radiata* is available, we therefore selected this last species to better understand the mechanisms of incompatibility mediated by SK48 by comparative transcriptomic analysis of the roots inoculated either by the WT strain DOA9 and its derivative Δ*SK48* mutants. Total RNA of SUT1 was extracted and purified from three treatments, including non-inoculation (NI), DOA9 WT inoculation, and Δ*SkP48* inoculation. Transcriptome analysis at the early stages of nodulation (4 dpi) was performed using next-generation sequencing (NGS). Several genes were induced in response to the NI, DOA9 WT, and Δ*SkP48* treatments, with substantial overlap in expression among the treatments (Figure 5). The number of genes differentially expressed genes significantly varied (P-value < 0.05, considering genes with fold change ≥ 1.5 as upregulated and fold change ≤ 0.67 as downregulated, with the expression of 2,185 DEGs being significant (1,311 upregulated DEGs and 874 downregulated DEGs) were identified from NGS. To identify only the *SkP48*-responsive DEGs in *V. radiata*, the Venn diagram was used. It was found that up-regulated DEGs was not observed in the comparison of NI vs Δ*SkP48* and NI vs DOA9 WT whereas the 65 and 350 down-regulated DEGs, respectively were identified. According to the comparison of DOA9 WT vs Δ*SkP48*, around 584 up-regulated DEGs and 411 down-regulated DEGs were identified in *V. radiata* (Figure 5A). The unique DEGs from DOA9 WT vs Δ*SkP48* were selected and analysed using Gene Ontology (GO) functional enrichment analysis for terms involving molecular functions, cellular components, and biological processes. Comparison of

188 the distribution of genes ($P_{adj} < 0.05$) for 30 GO terms in three ontologies between SUT1 plants
189 inoculated with DOA9 WT and Δ*SkP48* is shown in Figure 5B. Meanwhile, 102 KEGG
190 orthologies were assigned to the mapped sequences, with metabolic pathways being the most
191 assigned KEGG reference pathways (Figure 5C). Upregulated DEGs (DOA9 vs *ΔSK48*) were
192 associated with secondary cell wall biosynthesis, cell wall organisation, xylan biosynthetic
193 process, and others. Interestingly, several downregulated DEGs (DOA9 vs *ΔSK48*) were linked
194 to plant defence responses (Table S2), and 9 DEGs were annotated as defence response genes,
195 including two genes homologous to plant defensin (*PDF*) and one gene homolog to MLO-like
196 protein, DMR6 oxygenase 2, patatin, peamaclein, TIFY transcription, aminotransferase ALD1,
197 chalcone synthase (*CHS*), and thaumatin. ALD1 and MLO-like genes can trigger plant
198 immunity via salicylic acid metabolism [19,20]. Thaumatin-like protein 1, pathogenesis-related
199 protein 2 (*PR2*), and defensin, which are involved in plant immune responses against
200 pathogenic invasion, were downregulated [21,22]. These results suggest that DOA9 inhibits
201 symbiotic interactions with *V. radiata* SUT1 by triggering host immunity. *CHS*, a key enzyme
202 involved in the iso-flavonoid biosynthetic pathways, in mung bean roots was downregulated to
203 a lesser extent in response to *ΔSkP48* inoculation than in response to DOA9 WT inoculation.
204 *CHS* expression induces flavonoid and iso-flavonoid phytoalexin accumulation and is involved
205 in salicylic acid defence pathways [23].

206 To confirm the results of transcriptome analysis, the expression levels of eight DEGs, including
207 *PR5*, *PR2*, gibberellin 20 oxidase (*GA20ox*), linoleate lipoxygenase (*LOX*), calmodulin, *CHS*,
208 *PDF*, and auxin efflux carrier component (*PIN1*), were verified using qRT-PCR analysis
209 (Figure S2). *GA20ox* expression was upregulated (3-fold) in SUT1 plants inoculated with
210 Δ*SkP48* compared to that in plants inoculated with DOA9 WT, consistent with NGS data.
211 Meanwhile, *PR5*, *PR2*, *LOX*, *CHS*, defensin, and *PIN1* were downregulated (2–5-fold) in plants
212 inoculated with Δ*SkP48*. Only calmodulin showed no significant difference in expression

213 between SUT1 plants inoculated with Δ*SkP48* and DOA9 WT. Overall, the results of qRT-
214 PCR and NGS were consistent.

215 **Systemic acquired resistance (SAR)-related gene expression and salicylic acid content**

216 Based on the results of our transcriptome analysis and qRT-PCR verification, we hypothesized
217 that SkP48 suppresses SUT1 nodulation by triggering plant defence via salicylic acid signalling
218 and SAR-related gene expression in *Vigna*. The expression levels of SAR-related genes,
219 including *PR5*, *PR2*, *CHS*, pathogenesis-related gene transcriptional activator (*PTi5* and *PTi6*),
220 and non-race-specific disease resistance (*NDR1*), were analyzed upon DOA9 WT and Δ*SkP48*
221 inoculation in SUT1. At 4 dpi, the expression levels of all selected genes in Δ*SkP48*-inoculated
222 plants were lower (2–10-fold) than those in DOA9 WT-inoculated plants (Figure 6A).

223 To confirm that salicylic acid production is stimulated in roots after DOA9 inoculation, we
224 compared its content between DOA9 WT- and *ΔSkP48*-inoculated plants at 4 dpi (Figure 6B).
225 There was no difference in salicylic acid content between non-inoculated and *ΔSkP48*-
226 inoculated plants, while the salicylic acid content of DOA9-inoculated plants was significantly
227 higher (approximately 2-fold) than that of *ΔSkP48*-inoculated plants. These results suggest that
228 SkP48 promotes salicylic acid accumulation at the early stages of *V. radiata–Bradyrhizobium*
229 sp. DOA9 interaction.

230 ***Discussion***

231 Legume–rhizobium associations are specifically regulated by plant host and rhizobial factors,
232 and these may therefore not always be successful or efficient. For instance, DOA9 T3SS is one
233 of the factors controlling symbiotic properties [16,17]; however, there is limited information on
234 molecular mechanisms underlying the interactions between rhizobial DOA9 T3Es and legume
235 factors. In the DOA9 genome, 14 putative T3Es have been reported , 3 of them harboring a

small Ulp1 domain were predicted to belong to the family of C48 SUMO proteases Figure 1A) [16]. Several SUMO protease T3Es identified in various *Bradyrhizobium*s strain were already reported to mediate symbiotic incompatibility, such as BEL2-5 identified in *B. elkanii* USDA61 strain which blocks symbiosis with the soybean genotype Rj4 [24,25] or NopD identified in *Bradyrhizobium* SP. *XS1150* which negatively affects the nodulation of *Tephrosia vogelii* [9]. Among the three putative C48-SUMO proteases identified in the DOA9 genome, one (gene ID WP_025038828.1) harbors a unique SK domain. A T3E (mlr6331) identified in *Mesorhizobium loti* MAFF303099 strain containing an SK-like domain has been reported to be responsible for the T3SS-mediated blockage of symbiosis with *Lotus leucocephala* [26]. However, an effector containing in the same time a SK and a SUMO protease domain has not been yet reported. The results reported here, show that the putative effector, named SkP48, identified in the DOA9 genome is a novel type of T3E which is responsible of the incompatibility of the DOA9 strain with several legume species.

Specifically, SkP48 negatively regulated symbiosis with *V. radiata* and *V. mungo*, although these effects differ according the species (Figures 2, and Table S1). *Vigna* cultivars inoculated with Ω*rhcN* and *ΔSkP48* formed effective nodules, whereas those inoculated with DOA9 WT formed significantly fewer normal nodules (Table S1). Therefore, SkP48 may serve as the key T3E negatively regulating *Vigna–Bradyrhizobium* sp. DOA9 symbiosis. In addition, *ΔSkP48* significantly improved nodulation efficiency in *C. juncea* and *A. hypogea*. These results suggest that among the cocktail of T3Es secreted, SkP48 is most probably recognised by R-proteins, thereby inhibiting infection and/or nodulation to a greater or lesser extent. As previously mentioned, some SUMO proteases and SKs have been reported to act as negative T3Es in plant hosts [9,26–28], raising the possibility that DOA9 SkP48 responsible for this incompatibility can be either one or both protein domains (SUMO protease and/or SK domain). Therefore, this work builds a theoretical foundation for future research into the specific protein

261 domains within SkP48 that contribute mainly to the host immune responses. In contrast, the
262 Ω*rhcN* mutation reduced nodulation in *S. hamata*, while nodulation efficiency did not differ
263 between plants inoculated with DOA9 WT and *ΔSkP48* (Table S1). Therefore, other T3E(s)
264 may positively regulate symbiosis of DOA9 with other legumes species, perhaps by either
265 helping the bacteria to overcome plant defence or directly inducing nodulation signalling
266 pathways [13,29]. These results indicate that SkP48 plays pivotal roles in the suppression of
267 legume nodulation and that the DOA9 strain may be an ideal model to study the precise roles
268 of individual effectors. It is also to highlight that the SUMO protease Bel2-5 which is
269 responsible of the symbiotic incompatibility of USDA61 with Rj4 soybean genotype is in
270 counter part responsible of nodule induction in *G. max* cv. Enrie in the absence of NFs synthesis
271 [11]. We cannot therefore exclude that SkP48 could play also a positive symbiotic role on other
272 legume species.

273 Furthermore, SkP48 triggered the expression of some intermediate salicylic acid signalling-
274 related genes (*NDR1* and *CHS*). Interestingly, SkP48 also enhanced the biosynthesis of
275 salicylic acid, which governs plant defence responses (Figure 6). Moreover, in the incompatible
276 *Vigna* cultivar SUT1, SkP48 induced the expression of *PDF*, which is involved in plant
277 immune responses of the jasmonic acid pathway [22]. Based on these results, we propose a model
278 of DOA9 SkP48-mediated regulation of legume symbiosis, as shown in Figure 7. Since the
279 rhizobial T3E secretion signal is located in the N terminal, therefore N terminal region of SkP48
280 will further be performed to demonstrate whether SkP48 is indeed secreted via to the T3SS.
281 Thus, SkP48-tagged version (i.e. with HA tag) will be carried out, and protein will be detected
282 by Western blot analysis using the specific antibody from the supernatant of the
283 *Bradyrhizobium* sp. DOA9 wild type and a T3SS mutant (i.e. Ω*rhcN*) strains. In addition,
284 symbiotic phenotype of the SkP48 mutant is very strong. It points out that SkP48 is the main
285 responsible of the nodulation blockade in all those legumes. However, the gene encoding

SkP48 is very large (more than 9 kb), the complementation of whole gene is somewhat difficult, thus construction of a new independent mutant and perform at least one nodulation assay including both mutant strains will be conducted in order to determined which part of this large protein is recognized by the host plants.

In conclusion, the new putative T3E SkP48 is the key factor that suppresses nodulation and nodule organogenesis through the activation of effector-triggered immunity via salicylic acid biosynthesis induction, which is deleterious to rhizobial infection. In addition, nodulation likely interferes with the function of *PDF* in the jasmonic acid signalling pathway in *Vigna* SUT1.

Material and Methods

Bacterial strains, plasmids, and culture conditions

The bacterial strains and plasmids used in the present study are listed in Table S3. *Bradyrhizobium* sp. DOA9, and its derivative mutants were cultured at 28°C for 5 days in yeast mannitol (YM) medium [30]. *Escherichia coli* was grown at 37°C in Luria–Bertani (LB) medium [31]. The media were supplemented with antibiotics at the following concentrations: 200 μg·mL^{-1} streptomycin (Sm), 30 μg·mL^{-1} nalidixic acid (Nal), and 20 μg·mL^{-1} cefotaxime (cefo).

SkP48 mutant strain construction

A SkP48 clean deletion mutant was constructed by double crossing-over. For this purpose, the upstream and downstream flanking regions (~800 bp) of the *SkP48* (WP_025038828.1) gene was amplified using the primers Up-SkP48.D9.del.f/Up-SkP48.D9.del.r and Dw-SkP48.D9.del.f./Dw-SkP48.D9.del.r (Table S4). PCR fragments corresponding to the upstream and downstream flanking regions were merged using overlap extension PCR and cloned at the *Bam*HI/*Xba*I sites of *pK18mob-sabB-cefo^r* plasmid [32], which is non-replicative in *Bradyrhizobium* strains and which carries the cefotaxime resistance (*cefo*) and *sacB* genes. The

309 resulting plasmid was electroporated (15 kv cm^{-1}, 100 Ω, and 25 mF) into *E. coli* S17-1, and
310 the conjugate was transferred into the DOA9 strain using bi-parental mating [33]. A single
311 recombinant mutant was selected by growing the bacteria on plates containing 20 $\mu g \cdot mL^{-1}$ cefo
312 and subsequently verified using diagnostic PCR. The deletion mutant (double-recombinant
313 strain) was selected with a subsequent step in which the bacteria were grown on 10% sucrose
314 YM plates. The sucrose resistant and cefotaxime-sensitive clones were further screened for the
315 deletion of the corresponding genomic DNA region by PCR (Figure S3).

316 ***Plant nodulation and symbiosis analysis***

317 *Bradyrhizobium* sp. DOA9 and its derivatives (Table S3) were grown in YM medium at 30°C
318 for 5 days. A total of 13 *V. radiata* varieties were provided by Professor Piyada Alisha
319 Tantasawat. Among the *V. radiata* tested genotypes, 13 were Thai certified/published varieties
320 that are popularly cultivated by Thai farmers (KPS1, KPS2, SUT1, SUT2, SUT3, SUT4, SUT5,
321 CN36, CN72, CN84-1, M4-2, M5-1, and PSU-1) [10,34]. The study complies with local and
322 national regulations in Thailand. Seeds of all tested plants (Table S5) were sterilized as
323 previously described [14]. Two-day-old germinated seedlings were transplanted to Leonard's jars
324 (383 cm^3) containing sterilized vermiculite (single plant per plastic jar), and BNM medium [35]
325 (150 mL) was added to provide plant nutrients. At 5 days after transplanting, the seedlings were
326 inoculated with 1 mL of 4-day-old inoculum (10^8 CFU mL^{-1}). Six replicates were set per
327 treatment as follows: non-inoculation (NI), wild type (DOA9), *rhcN* mutant strain (*ΩrhcN*) [16],
328 and *SkP48* mutant strain (*ΔSkP48*). The plants were cultivated under controlled environmental
329 conditions of 28 ± 2°C with a 16/8-h day/night regimen at 300 $\mu E\ m^{-2}\ S^{-1}$ light intensity and
330 50% humidity. The plants were harvested after 30 days post inoculation (dpi), and dry weight
331 of the whole plant and nodule number were measured. Furthermore, nodule sections were
332 examined, and nitrogenase activity was determined using the acetylene reduction assay (ARA)
333 [36].

334 ***Microscopy***

335 Bacterial morphology was observed using the Olympus Fluoview FV1000 confocal laser
336 scanning microscope (Japan), and 40–50-μm-thick nodule sections were prepared using a
337 vibratome (VT1000S, Leica Nanterre, France). Bacteria were then stained with live/dead
338 staining solution (5 μM SYTO9 and 30 μM propidium iodide in 50 mM Tris [pH 7.0] buffer;
339 Live/Dead BacLight, Invitrogen, Carlsbad, CA, USA) for 15 min. The sections were washed
340 with 10 mM phosphate saline buffer, and the plant cell walls were stained for additional 15
341 min in 10 mM phosphate saline buffer containing calcofluor white M2R (Sigma, Munich,
342 Germany) at a final concentration of 0.01% (w/v) [37]. Calcofluor was excited at 405 nm and
343 detected using a 460–500 nm emission filter. SYTO9 was excited with the 488 nm laser line,
344 and emission signals were collected at 490–522 nm. PI was excited with the 535 nm laser line,
345 and emission signals were collected at 617–636 nm. Confocal images were reconstructed using
346 Nikon NIS-Elements.

347 ***Bacterial RNA isolation and qRT-PCR***

348 The mid-log phase culture of DOA9 was washed, and OD_{600} was adjusted to approximately 0.4
349 using AG medium [30] supplemented with purified flavonoids (20 μM genistein dissolved in
350 DMSO). DMSO alone was used as the negative control. Bacterial cells were cultured at 28°C
351 for 16 h, collected by centrifugation (4,000 rpm for 10 min at 4°C), and immediately frozen in
352 liquid nitrogen prior to storage at −80°C for further total RNA isolation.

353 Total bacterial RNA was extracted from induced cells using the RNeasy Mini Kit (Qiagen,
354 USA) according to the manufacturer's protocol. The extracted RNA was treated with RNase-
355 free DNase I (NEB, USA) for 30 min at 37°C, and cDNA was synthesized from 500 ng of total
356 RNA using the High-Capacity cDNA Reverse Transcription Kit (iScript, Bio-Rad, USA)
357 according to the manufacturer's protocol. The synthesized cDNA (25 ng) was subjected to PCR

amplification with gene-specific primers (Table S4) using the QuantStudio 3 Real-Time PCR System Mix (Applied Biosystems, USA). The PCR program included an initial denaturation step at 95°C for 2 min, followed by 40 cycles at 95°C for 30 s, 55°C for 30 s, and 72°C for 30 s, and a final extension step at 72°C for 10 min. Relative gene expression was calculated using the comparative Ct (-ΔΔCT) method [38] and normalized to the expression of the endogenous housekeeping gene 16S rRNA (Table S4). Data from three biological replicates were pooled and analyzed. At least three PCR amplifications were performed for each sample.

Transcriptome analysis of V. radiata

For RNA sequencing (RNA-Seq) of *V. radiata* roots, seeds were surface sterilized, germinated at 25°C for 2 days, and transplanted to Leonard's jars containing BNM medium. After germination for 3 days, the plants were inoculated with bacterial cultures (2×10^7 cells·mL^{-1}, three biological replicates per sample). At 4 dpi, *V. radiata* roots were immediately frozen in liquid nitrogen and ground to a fine powder. Next, 100 mg of the powder was used for total RNA extraction using the RNeasy Plant Mini Kit (Qiagen, USA) and treated with DNase I (Qiagen, USA) according to manufacturer's instructions. A cDNA library was constructed from 4 μg of total RNA using the TruSeq Stranded mRNA LT Sample Prep Kit (Illumina, USA) following the manufacturer's protocol. Each library was sequenced using the Illumina platform and subjected to bioinformatics at GENEWIZ (Suzhou, China). Differentially expressed genes (DEGs) were selected for further analysis based on *P*-value < 0.01, considering genes with fold change ≥ 1.5 as upregulated and fold change ≤ 0.67 as downregulated. The datasets of DEGs (linked to plant defence responses) for this study can be found in the Table S2 and accession ID of NGSs is ID: SUB10069088.

qRT-PCR of DEGs

Selected DEGs were subjected to qRT-PCR using the same protocol as above. The primer sets used for qRT-PCR are listed in Table S4. The transcript levels of selected *V. radiata* DEGs were normalized to the expression of the housekeeping gene *β-actin* as previously mentioned [39–44].

Measurement of salicylic acid content

For quantifying the salicylic acid content of *V. radiata* roots, seeds were surface sterilized, germinated at 25°C for 2 days, and transplanted to Leonard's jars containing BNM medium. Five days after transplantation, the plants were inoculated with bacterial cultures (2×10^7 cells·mL^{-1}). At 4 dpi, *V. radiata* roots were collected and ground to a fine powder in liquid nitrogen. Next, 1 mL of 90% methanol was added to 100 mg of the powder. The mixture was homogenized using a blender for 2 min at 6,000 rpm, incubated overnight at 4°C, and centrifuged at 1,204 ×*g* for 10 min at 4 °C. The supernatant was collected, evaporated to dryness with a gentle stream of nitrogen, and resuspended in 20 µL of trichloroacetic acid (1 M). The suspension was partitioned three times against cyclohexane:ethyl acetate (1:1), and the organic phase was collected and dried in nitrogen. The dried organic phase of the root extract was reconstituted with 500 µL of methanol and filtered through a 0.22 µm PTFE membrane prior to high-performance liquid chromatography with a diode array detector (HPLC-DAD). The separations were performed on the Hypersil GOLD C18 column (100 mm × 2.1 mm i.d., 1.9 µm; Thermo Scientific, USA) at 30°C [45].

Statistical analysis

For phylogenetic and evolutionary analyses, SkP48 homologs were queried using BLASTx against genomic databases of bacterial species, including rhizobial and pathogenic bacteria. A phylogenetic tree was constructed using the neighbour-joining method based on the Poisson model in MEGA 7.0, with 1,000 bootstrap replications. The protein domains were

405 independently modelled using I-TASSER [46], assembled using DEMO [47], and visualized using
406 PyMOL 2.5.0. For statistical analyses, one-way analysis of variance (ANOVA) followed by
407 Tukey's post hoc test ($P \leq 0.05$) was performed using Minitab version 16.0 for multiple test
408 sample comparisons. Two-tailed Student's *t*-test was performed for pairwise comparison as
409 required. Statistical significance was set at $P < 0.05$. The sample size and replicates are detailed
410 in figure and table legends.

411 ***Acknowledgements***

412 This work was financially supported by the Suranaree University of Technology (SUT);
413 National Research Council of Thailand (NRCT)/Office of the Higher Education Commission
414 (OHEC)/The Thailand Research Fund project (TRG6280006); the Thailand Science Research
415 and Innovation (TSRI); the Office of National Higher Education Science Research and
416 Innovation Policy Council (nxpo) by the Program Management Unit (PMU-B) project
417 (B05F630107); IRD (JEAI_SymbiTrop) and by the ANR grants 'SymEffectors' and 'ET-Nod'
418 number ANR- 16-CE20-0013 and ANR-20-CE20-0012, respectively.

419 ***Figure Legends***

420 **Figure 1.** Schematic representation of the new putative effector protein SkP48 harboring the
421 shikimate kinase and C48 SUMO protease domains in DOA9 (A). (B) Schematic
422 representation of SkP48 functional domains in DOA9, in comparison to its homologs in
423 rhizobia and pathogenic bacteria. The repeat domains are showed in different colors [internal
424 repeat domain (RPT) in grey, shikimate kinase domain (SK) in yellow, and ULP1 domain in
425 blue]. (C) Expression of putative T3E SkP48 in *Bradyrhizobium* sp. DOA9 (DOA9) and its
426 T3SS mutant strain (Ω*rhcN*) in presence or absence of genistein inducer. Data are presented as
427 means ± standard deviations. Different letters indicate significant differences at $P < 0.05$.

428 **Figure 2.** Symbiotic nodulation of *Bradyrhizobium* sp. DOA9 and its mutant derivatives in
429 *Vigna radiata* cv. SUT1. Cytological aspect of nodules (A-C) at 10 dpi: A (DOA9), B (*ΩrhcN*),

and C (*ΔSkP48*); (D-F) 15 dpi: D (DOA9), E (*ΩrhcN*), and F (*ΔSkP48*); and (G-I) 30 dpi: G (DOA9), H (*ΩrhcN*), and I (*ΔSkP48*). Bar = 1 mm. Propidium iodide (PI) and SYTO9 staining of sectioned nodules (J-L): J (WT), K (*ΩrhcN*), and L (Δ*SkP48*). Total nodule number per plant (M), ARA activity (N), and plant dry weight (O) were determined at 30 dpi. "*", $P < 0.05$ and "**", $P < 0.01$ according to Student's *t*-test. The means followed by different letters are significantly different at the 5% level ($P \leq 0.05$ according to Tukey's test) (n=6).

Symbiotic nodulation of *Bradyrhizobium* sp. DOA9 and its mutant derivatives in *Vigna mungo*. Cytological aspect of root nodules (P-R): P (DOA9), Q (*ΩrhcN*), and R (*ΔSkP48*). Bar = 1 mm. Propidium iodide (PI) and SYTO9 staining of sectioned nodules (S-U): S (WT), T (*ΩrhcN*), and U (Δ*SkP48*). Total nodule number per plant (V), ARA activity (W), and plant dry weight (X) were determined at 30 dpi. The means followed by different letters are significantly different at the 5% level ($P \leq 0.05$ according to Tukey's test) (n=6).

Figure 3. Symbiotic nodulation of *Bradyrhizobium* sp. DOA9 and its mutant derivatives in *Crotalaria juncea*. Cytological aspect of roots (A-C): A (DOA9), B (*ΩrhcN*), and C (*ΔSkP48*); bar = 1 cm. Nodule morphology (D-F): D (DOA9), E (*ΩrhcN*), and F (*ΔSkP48*). Bar = 1 mm. Propidium iodide (PI) and SYTO9 staining of sectioned nodules (G-I): G (WT), H (*ΩrhcN*), and I (ΔSkP48). Total nodule number per plant (J), ARA activity (K) and, plant dry weight (L) were determined at 30 dpi. The means followed by different letters are significantly different at the 5% level ($P \leq 0.05$ according to Tukey's test) (n=6).

Figure 4. Symbiotic nodulation of *Bradyrhizobium* sp. DOA9 and its mutant derivatives in *Arachis hypogea*. Cytological aspect of roots (A-C): A (DOA9), B (*ΩrhcN*), and C (*ΔSkP48*). Bar = 1 cm. Nodule morphology (D-F): D (DOA9), E (*ΩrhcN*), and F (*ΔSkP48*). Bar = 1 mm. Propidium iodide (PI) and SYTO9 staining of sectioned nodules (G-I): G (WT), H (*ΩrhcN*), and I (ΔSkP48). Total nodule number per plant (J), ARA activity (K) and, plant dry weight (L)

were determined at 30 dpi. The means followed by different letters are significantly different at the 5% level ($P \leq 0.05$ according to Tukey's test) (n=6).

Figure 5. Differentially expressed genes (DEGs) in *Vigna radiata* cv. SUT1 inoculated with DOA9 *versus ΔSkP48*. (A) Venn diagram showing the number of unique DEGs (upregulated and downregulated genes) in each or multiple treatment groups: non-inoculation (NI), DOA9 wild-type inoculation (DOA9), and SkP48 mutant strain inoculation (*ΔSkP48*). Functional analysis of DGEs in DOA9 *versus ΔSkP48* treatment: (B) GO and (C) KEGG enrichment of DEGs.

Figure 6. qRT-PCR results of gene expression in *Vigna radiata* cv. SUT1 inoculated with DOA9 and *ΔSkP48* at 4 dpi. (A) Expression levels of differentially expressed genes in SUT1: chalcone synthase (*CHS*), non-disease resistance 1 (*NDR1*), pathogenesis-related genes transcriptional activator 5 (*PTi5*), pathogenesis-related genes transcriptional activator 6 (*PTi6*), pathogenesis-related protein 2 (*PR2*), and pathogenesis-related protein 5 (*PR*5). (B) Salicylic acid content of *V. radiata* roots: non-inoculation (NI), DOA9 inoculation (DOA9), and SkP48 mutant strain (*ΔSkP48*) inoculation. Results were derived from triplicate experiments. Asterisks indicate significant differences at $P < 0.05$.

Figure 7. Putative model of host genotype-specific symbiotic interactions between *Bradyrhizobium* sp. DOA9 and legumes controlled by the new putative T3E SkP48. Hypothetically, SkP48 is one of the nodulation determinants that inhibits the nodulation of *Vigna* varieties, *Crotalaria juncea*, and *Arachis hypogea*, possibly through promoting the phytohormone-mediated effector-triggered immunity (PmETI-type) of host. SkP48 might be recognized by unknown receptor(s) or a specific resistance (R) protein in the legumes, consequently activating an R protein-mediated ETI-type defence response (RmETI-type) to inhibit nodulation. Dotted line indicates unclear symbiotic mechanisms.

References

1. Oldroyd, G. E. D., Murray, J. D., Poole, P. S. & Downie, J. A. The rules of engagement in the legume-rhizobial symbiosis. *Annu. Rev. Genet.* **45**, 119–144 (2011).

2. Roy, S. *et al.* Celebrating 20 Years of Genetic Discoveries in Legume Nodulation and Symbiotic Nitrogen Fixation. *Plant Cell* **32**, 15–41 (2020).

3. Gibson, K. E., Kobayashi, H. & Walker, G. C. Molecular determinants of a symbiotic chronic infection. *Annu. Rev. Genet.* **42**, 413–441 (2008).

4. Janczarek, M., Rachwał, K., Marzec, A., Grzadziel, J. & Palusińska-Szysz, M. Signal molecules and cell-surface components involved in early stages of the legume-rhizobium interactions. *Appl. Soil Ecol.* **85**, 94–113 (2015).

5. Viprey, V., Del Greco, A., Golinowski, W., Broughton, W. J. & Perret, X. Symbiotic implications of type III protein secretion machinery in *Rhizobium*. *Mol. Microbiol.* **28**, 1381–1389 (1998).

6. Krause, A., Doerfel, A. & Göttfert, M. Mutational and transcriptional analysis of the type III secretion system of *Bradyrhizobium japonicum*. *Mol. Plant-Microbe Interact.* **15**, 1228–1235 (2002).

7. Bartsev, A. V. *et al.* NopL, an Effector Protein of *Rhizobium* sp. NGR234, Thwarts Activation of Plant Defense Reactions. *Plant Physiol.* **134**, 871–879 (2004).

8. López-Baena, F. J. *et al.* The absence of nops secretion in *Sinorhizobium fredii* HH103 increases GmPR1 expression in williams soybean. *Mol. Plant-Microbe Interact.* **22**, 1445–1454 (2009).

9. Xiang, Q. W. *et al.* NopD of *Bradyrhizobium* sp. XS1150 Possesses SUMO Protease Activity. *Front. Microbiol.* **11**, 1–12 (2020).

10. Piromyou, P., Nguyen, H. P., Songwattana, P. & Boonchuen, P. The *Bradyrhizobium diazoefficiens* type III effector NopE modulates the regulation of plant hormones towards nodulation in *Vigna radiata*. 1–12 (2021).

11. Okazaki, S., Kaneko, T., Sato, S. & Saeki, K. Hijacking of leguminous nodulation signaling by the rhizobial type III secretion system. *Proc. Natl. Acad. Sci. U. S. A.* **110**, 17131–17136 (2013).

12. Jiménez-Guerrero, I. *et al.* The *Sinorhizobium* (Ensifer) *fredii* HH103 type 3 secretion system suppresses early defense responses to effectively nodulate soybean. *Mol. Plant-Microbe Interact.* **28**, 790–799 (2015).

13. Ratu, S. T. N. *et al.* Rhizobia use a pathogenic-like effector to hijack leguminous nodulation signalling. *Sci. Rep.* **11**, 1–15 (2021).

14. Teamtisong, K. *et al.* Divergent Nod-containing *Bradyrhizobium* sp. DOA9 with a megaplasmid and its host range. *Microbes Environ.* **29**, 370–376 (2014).

15. Okazaki, S. *et al.* Genome analysis of a novel *Bradyrhizobium* sp. DOA9 carrying a symbiotic plasmid. *PLoS One* **10**, 1–18 (2015).

16. Songwattana, P. *et al.* Type 3 secretion system (T3SS) of *Bradyrhizobium* sp. DOA9 and its roles in legume symbiosis and rice endophytic association. *Front. Microbiol.* **8**, 1–12 (2017).

17. Piromyou, P. *et al.* Mutualistic co-evolution of T3SSs during the establishment of symbiotic relationships between *Vigna radiata* and Bradyrhizobia. *Microbiologyopen* **8**, (2019).

18. Li, S. J. & Hochstrasser, M. The Ulp1 SUMO isopeptidase: Distinct domains required

523 for viability, nuclear envelope localization, and substrate specificity. *J. Cell Biol.* **160**,
524 1069–1081 (2003).

525 19. Jong, T. S., Lu, H., McDowell, J. M. & Greenberg, J. T. A key role for ALD1 in
526 activation of local and systemic defenses in Arabidopsis. *Plant J.* **40**, 200–212 (2004).

527 20. van Butselaar, T. & Van den Ackerveken, G. Salicylic Acid Steers the Growth–
528 Immunity Tradeoff. *Trends in Plant Science* vol. 25 566–576 (2020).

529 21. Hayashi, M. *et al.* A thaumatin-like protein, Rj4, controls nodule symbiotic specificity
530 in soybean. *Plant Cell Physiol.* **55**, 1679–1689 (2014).

531 22. Serrazina, S., Machado, H., Costa, R. L. & Duque, P. Allene Oxide Synthase in
532 Arabidopsis Improves the Defense to *Phytophthora cinnamomi*. **12**, 1–15 (2021).

533 23. Dao, T. T. H., Linthorst, H. J. M. & Verpoorte, R. Chalcone synthase and its functions
534 in plant resistance. *Phytochem. Rev.* **10**, 397–412 (2011).

535 24. Faruque, O. M. *et al.* Identification of *Bradyrhizobium elkanii* genes involved in
536 incompatibility with soybean plants carrying the Rj4 allele. *Appl. Environ. Microbiol.*
537 **81**, 6710–6717 (2015).

538 25. Tsurumaru, H. *et al.* A putative type III secretion system effector encoded by the
539 MA20_12780 gene in *Bradyrhizobium japonicum* Is-34 causes incompatibility with
540 Rj4 genotype soybeans. *Appl. Environ. Microbiol.* **81**, 5812–5819 (2015).

541 26. Sanchez, C., Iannino, F., Deakin, W. J., Ugalde, R. A. & Lepek, V. C. Characterization
542 of the *Mesorhizobium loti* MAFF303099 type-three protein secretion system. *Mol.*
543 *Plant-Microbe Interact.* **22**, 519–528 (2009).

544 27. Okazaki, S. *et al.* Identification and functional analysis of type III effector proteins in

Mesorhizobium loti. *Mol. Plant-Microbe Interact.* **23**, 223–234 (2010).

28. Wang, J. *et al.* QTL Mapping and Data Mining to Identify Genes Associated With the *Sinorhizobium fredii* HH103 T3SS Effector NopD in Soybean. *Front. Plant Sci.* **11**, 1–16 (2020).

29. Okazaki, S. *et al. Rhizobium*-legume symbiosis in the absence of Nod factors: Two possible scenarios with or without the T3SS. *ISME J.* **10**, 64–74 (2016).

30. Sadowsky, M. J., Tully, R. E., Cregan, P. B. & Keyser, H. H. Genetic Diversity in *Bradyrhizobium japonicum* Serogroup 123 and Its Relation to Genotype-Specific Nodulation of Soybean. *Appl. Environ. Microbiol.* **53**, 2624–2630 (1987).

31. Wood, E. Molecular Cloning. A Laboratory Manual. *Biochem. Educ.* **11**, 82 (1983).

32. Songwattana, P. *et al.* Symbiotic properties of a chimeric Nod-independent photosynthetic *Bradyrhizobium* strain obtained by conjugative transfer of a symbiotic plasmid. *Environmental Microbiology* vol. 21 3442–3454 (2019).

33. Giraud, E., Lavergne, J. & Verméglio, A. Characterization of Bacteriophytochromes from Photosynthetic Bacteria: Histidine Kinase Signaling Triggered by Light and Redox Sensing. *Methods Enzymol.* **471**, 135–159 (2010).

34. Somta, P., Sommanas, W. & Srinives, P. Molecular diversity assessment of AVRDC-The World Vegetable Center elite-parental mungbeans. *Breed. Sci.* **59**, 149–157 (2009).

35. Ehrhardt, D. W., Morrey Atkinson, E. & Long, S. R. Depolarization of alfalfa root hair membrane potential by *Rhizobium meliloti* nod factors. *Science (80-.).* **256**, 998–1000 (1992).

567 36. Piromyou, P. *et al.* Effect of plant growth promoting rhizobacteria (PGPR) inoculation
568 on microbial community structure in rhizosphere of forage corn cultivated in Thailand.
569 *Eur. J. Soil Biol.* **47**, (2011).

570 37. Nagata, T. & Takebe, I. Cell wall regeneration and cell division in isolated tobacco
571 mesophyll protoplasts. *Planta* **92**, 301–308 (1970).

572 38. Livak, K. J. & Schmittgen, T. D. Analysis of relative gene expression data using real-
573 time quantitative PCR and the 2-ΔΔCT method. *Methods* **25**, 402–408 (2001).

574 39. Narancio, R., John, U., Mason, J. & Spangenberg, G. Selection of optimal reference
575 genes for quantitative RT-PCR transcript abundance analysis in white clover
576 (*Trifolium repens* L.). *Funct. Plant Biol.* **45**, 737–744 (2018).

577 40. Chi, C. *et al.* Selection and validation of reference genes for gene expression analysis
578 in *Vigna angularis* using quantitative real-time RT-PCR. *PLoS One* **11**, 1–13 (2016).

579 41. Ke, X. W. *et al.* Reference genes for quantitative real-time PCR analysis of gene
580 expression in mung bean under abiotic stress and *Cercospora canescens* infection.
581 *Legum. Res.* **44**, 646–651 (2021).

582 42. Kundu, A., Patel, A. & Pal, A. Defining reference genes for qPCR normalization to
583 study biotic and abiotic stress responses in *Vigna mungo*. *Plant Cell Rep.* **32**, 1647–
584 1658 (2013).

585 43. Dasgupta, U. *et al.* Comparative RNA-Seq analysis unfolds a complex regulatory
586 network imparting yellow mosaic disease resistance in mungbean [*Vigna radiata* (L.)
587 R. Wilczek]. *PLoS One* **16**, 1–24 (2021).

588 44. Bjarnadottir, H. & Jonsson, J. J. A rapid real-time qRT-PCR assay for ovine β-actin

589 mRNA. *J. Biotechnol.* **117**, 173–182 (2005).

590 45. Ji, R. *et al.* The Salicylic Acid Signaling Pathway Plays an Important Role in the
591 Resistant Process of *Brassica rapa* L. ssp. pekinensis to *Plasmodiophora brassicae*
592 Woronin. *J. Plant Growth Regul.* **40**, 405–422 (2021).

593 46. Yang, J. & Zhang, Y. I-TASSER server: New development for protein structure and
594 function predictions. *Nucleic Acids Res.* **43**, W174–W181 (2015).

595 47. Zhou, X., Hu, J., Zhang, C., Zhang, G. & Zhang, Y. Assembling multidomain protein
596 structures through analogous global structural alignments. *Proc. Natl. Acad. Sci. U. S.*
597 *A.* **116**, 15930–15938 (2019).

598

599

600

601

602

603

604

605

606

607

608

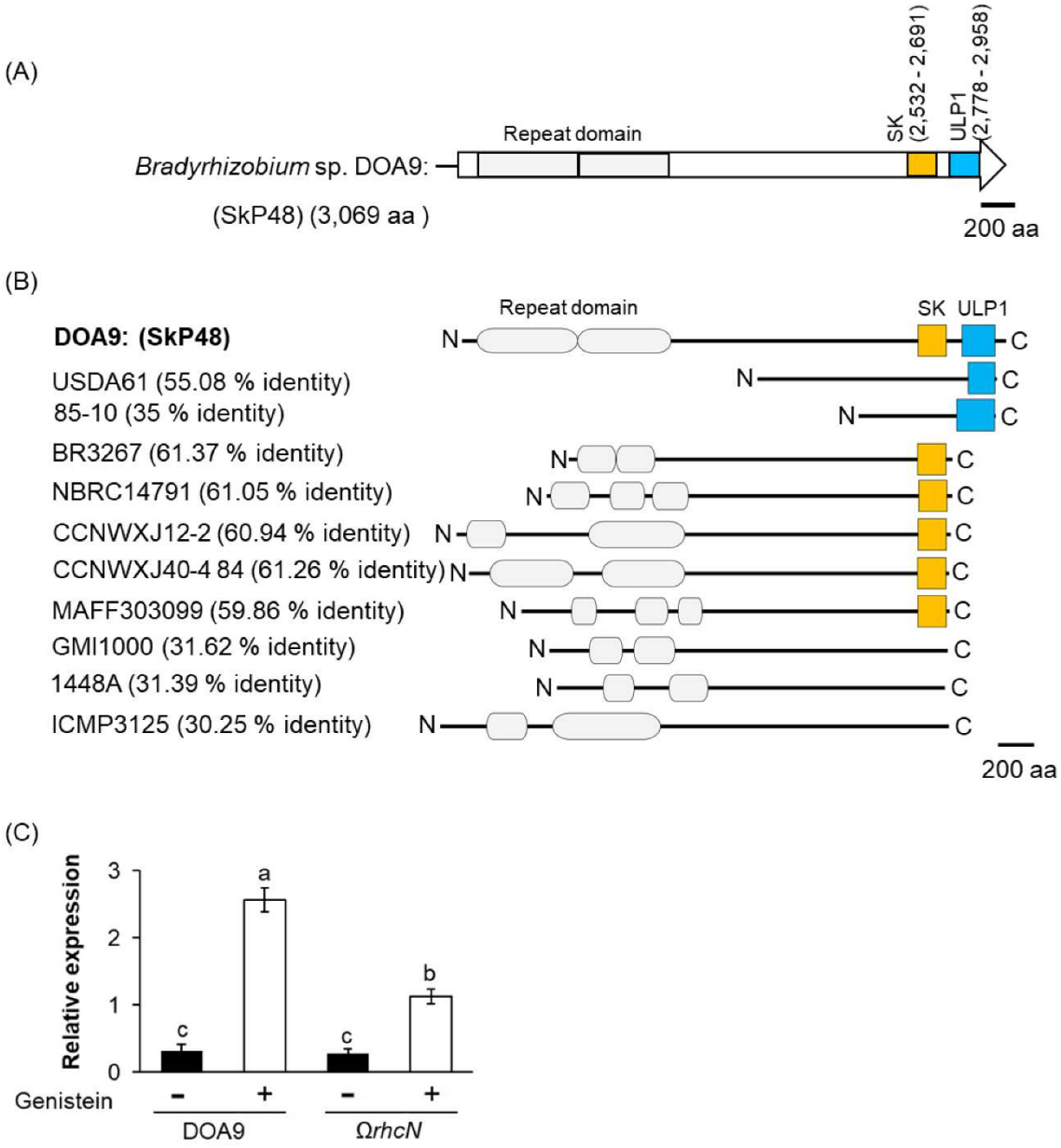
(A)
Repeat domain
SK (2,532 - 2,691)
ULP1 (2,778 - 2,958)
Bradyrhizobium sp. DOA9:
(SkP48) (3,069 aa)
200 aa
(B)
Repeat domain
SK
ULP1
DOA9: (SkP48)
USDA61 (55.08 % identity)
85-10 (35 % identity)
BR3267 (61.37 % identity)
NBRC14791 (61.05 % identity)
CCNWXJ12-2 (60.94 % identity)
CCNWXJ40-4 84 (61.26 % identity)
MAFF303099 (59.86 % identity)
GMI1000 (31.62 % identity)
1448A (31.39 % identity)
ICMP3125 (30.25 % identity)
N
C
200 aa
(C)
Relative expression
3
2
1
0
a
b
c
c
Genistein
-
+
-
+
DOA9
ΩrhcN

Figure 1

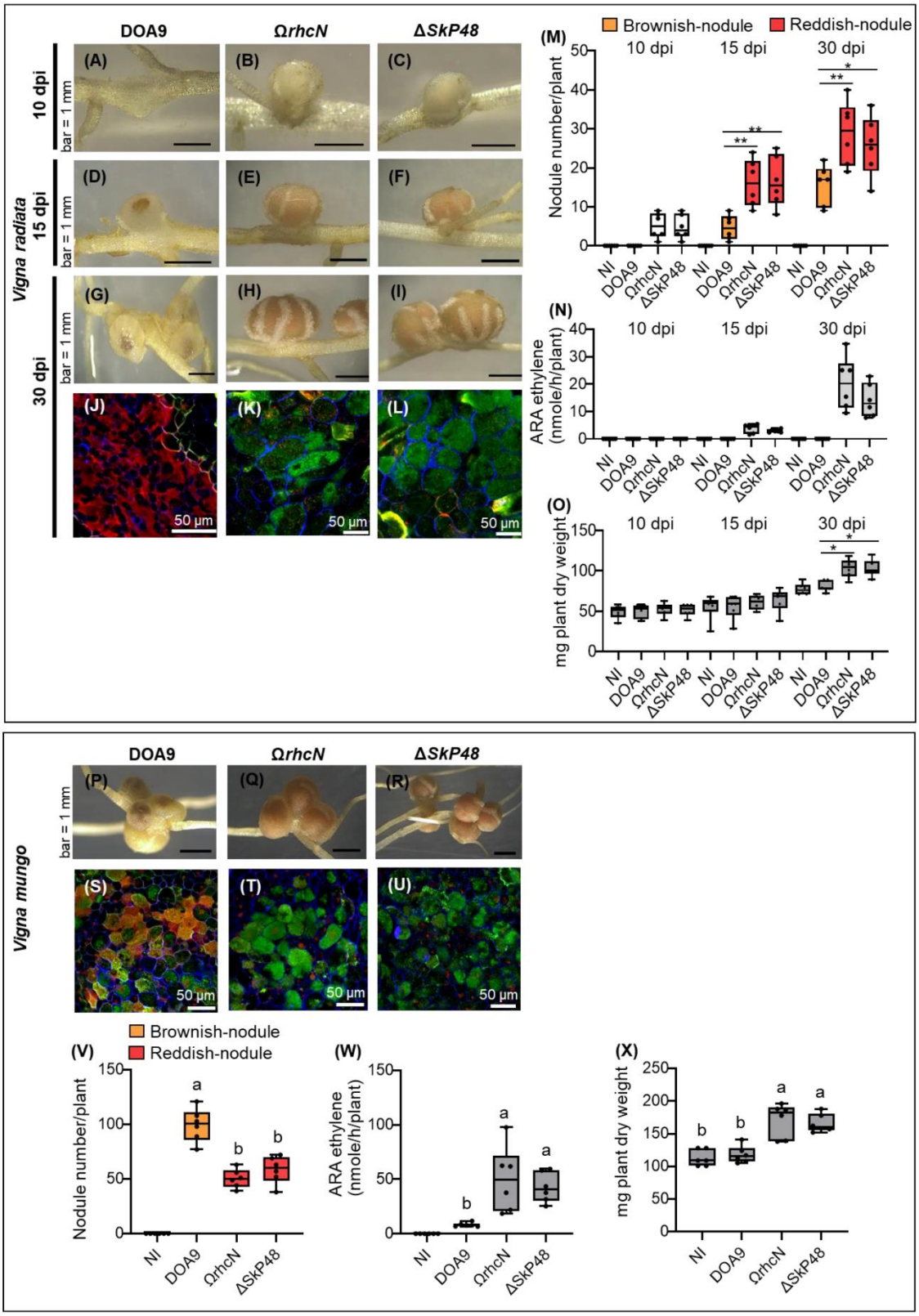

615

616 Figure 2

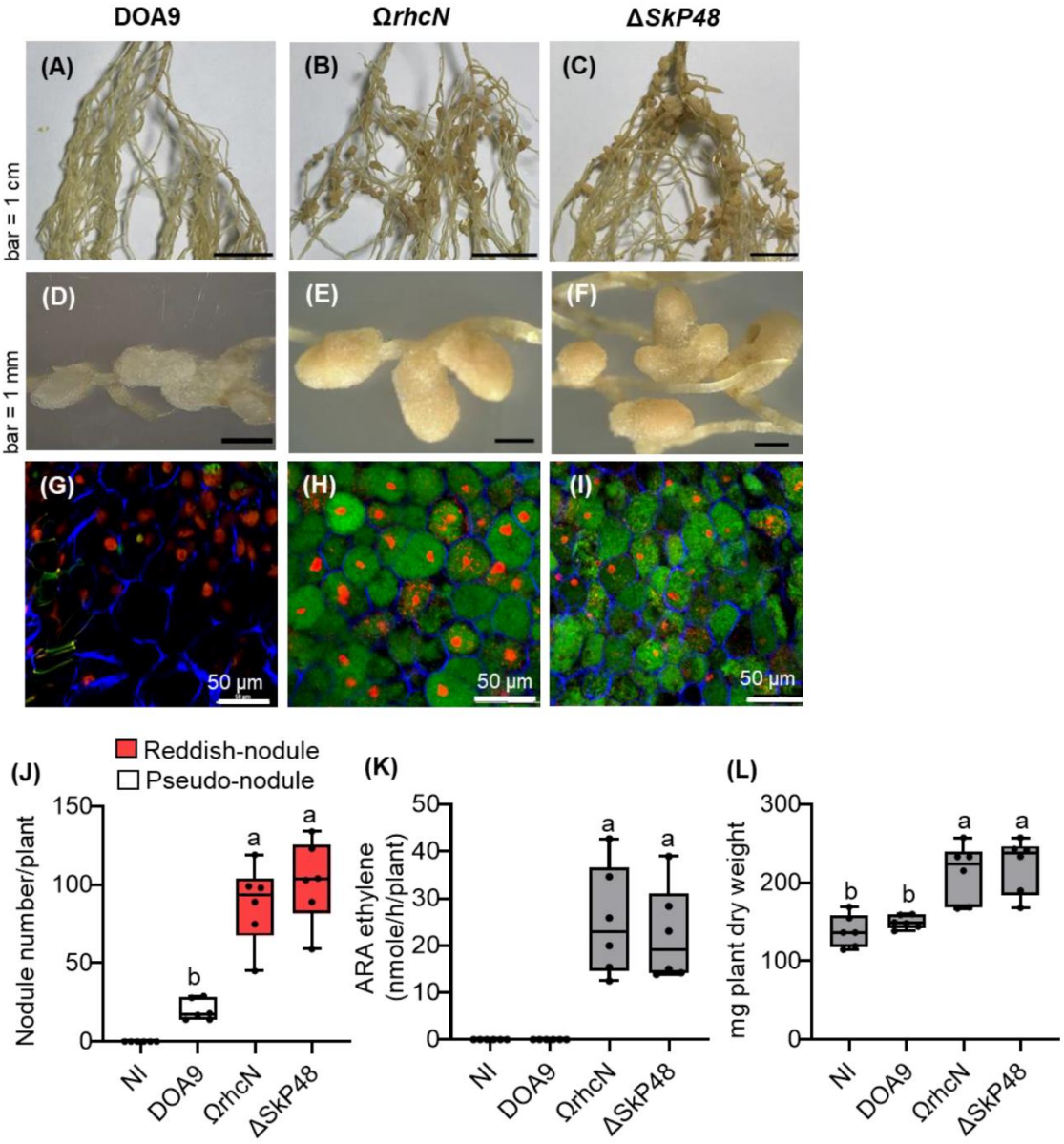
DOA9
ΩrhcN
ΔSkP48
(A)
(B)
(C)
bar = 1 cm
(D)
(E)
(F)
bar = 1 mm
(G)
(H)
(I)
50 µm
50 µm
50 µm
Reddish-nodule
Pseudo-nodule
(J)
Nodule number/plant
150
100
50
0
a
a
b
(K)
ARA ethylene (nmole/h/plant)
50
40
30
20
10
0
a
a
(L)
mg plant dry weight
300
200
100
0
a
a
b
b
NI
DOA9
ΩrhcN
ΔSkP48

Figure 3

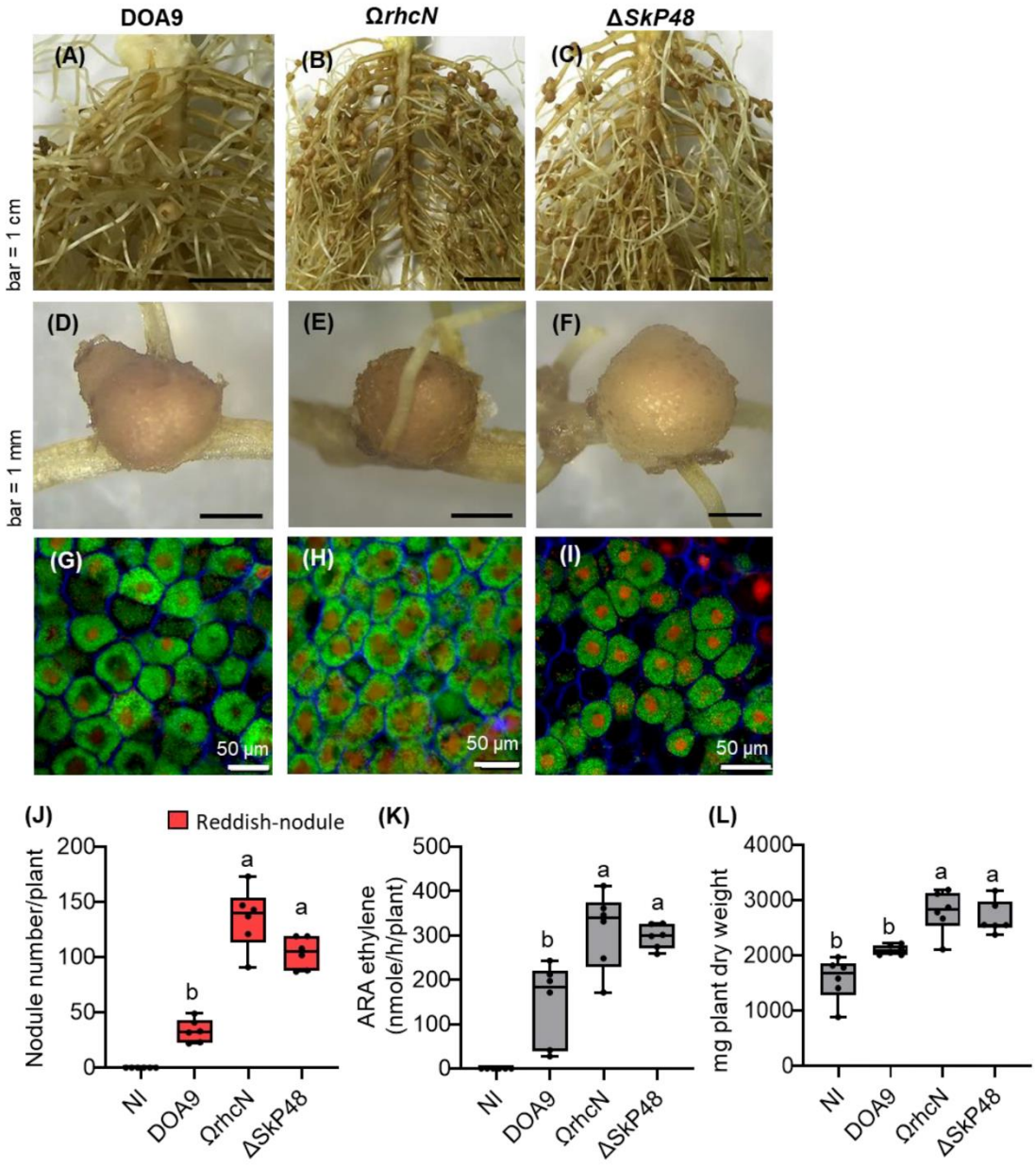
DOA9
ΩrhcN
ΔSkP48
(A)
(B)
(C)
bar = 1 cm
(D)
(E)
(F)
bar = 1 mm
(G)
(H)
(I)
50 µm
50 µm
50 µm
(J)
Reddish-nodule
Nodule number/plant
200
150
100
50
0
a
a
b
NI
DOA9
ΩrhcN
ΔSkP48
(K)
ARA ethylene (nmole/h/plant)
500
400
300
200
100
0
a
a
b
NI
DOA9
ΩrhcN
ΔSkP48
(L)
mg plant dry weight
4000
3000
2000
1000
0
a
a
b
b
NI
DOA9
ΩrhcN
ΔSkP48

Figure 4

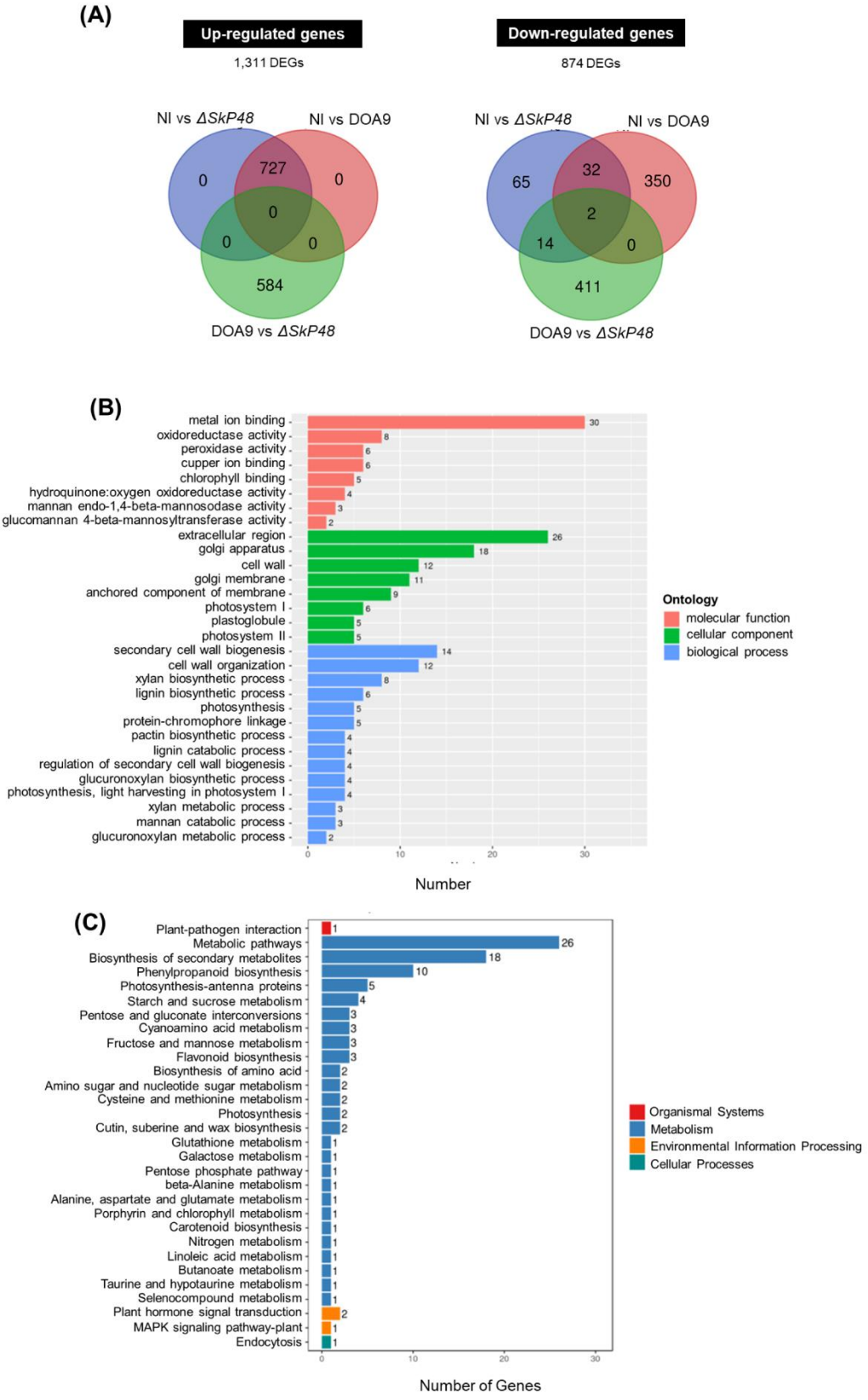

629

630 Figure 5

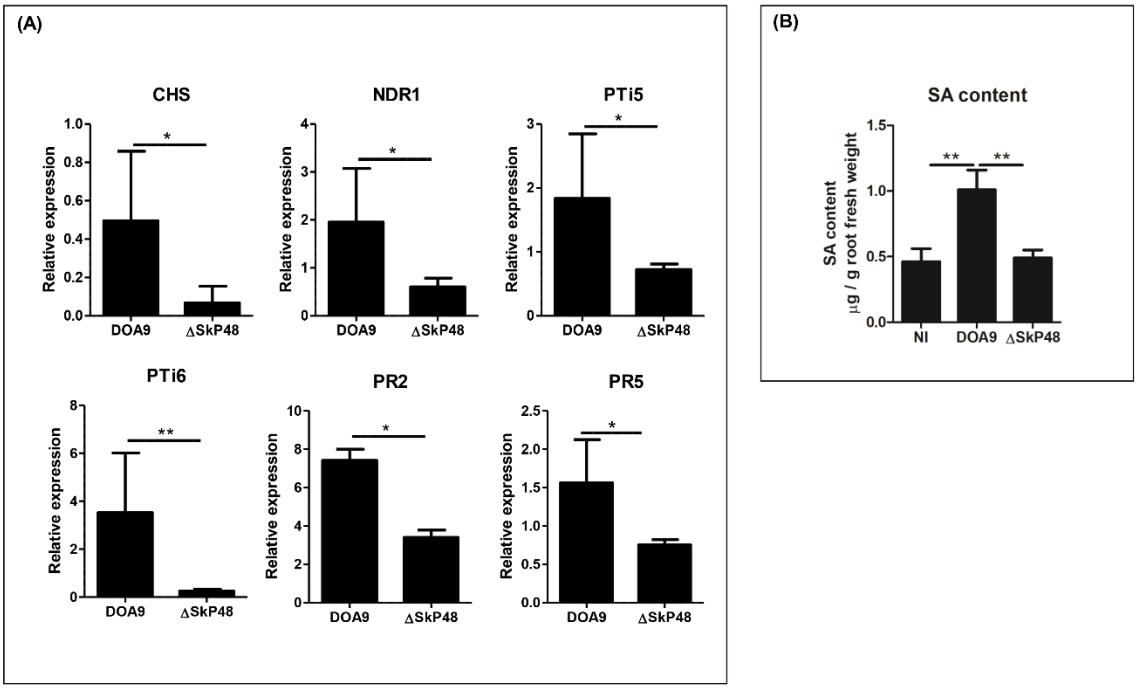

631

632

633 Figure 6

634

635

636

637

638

639

640

641

642

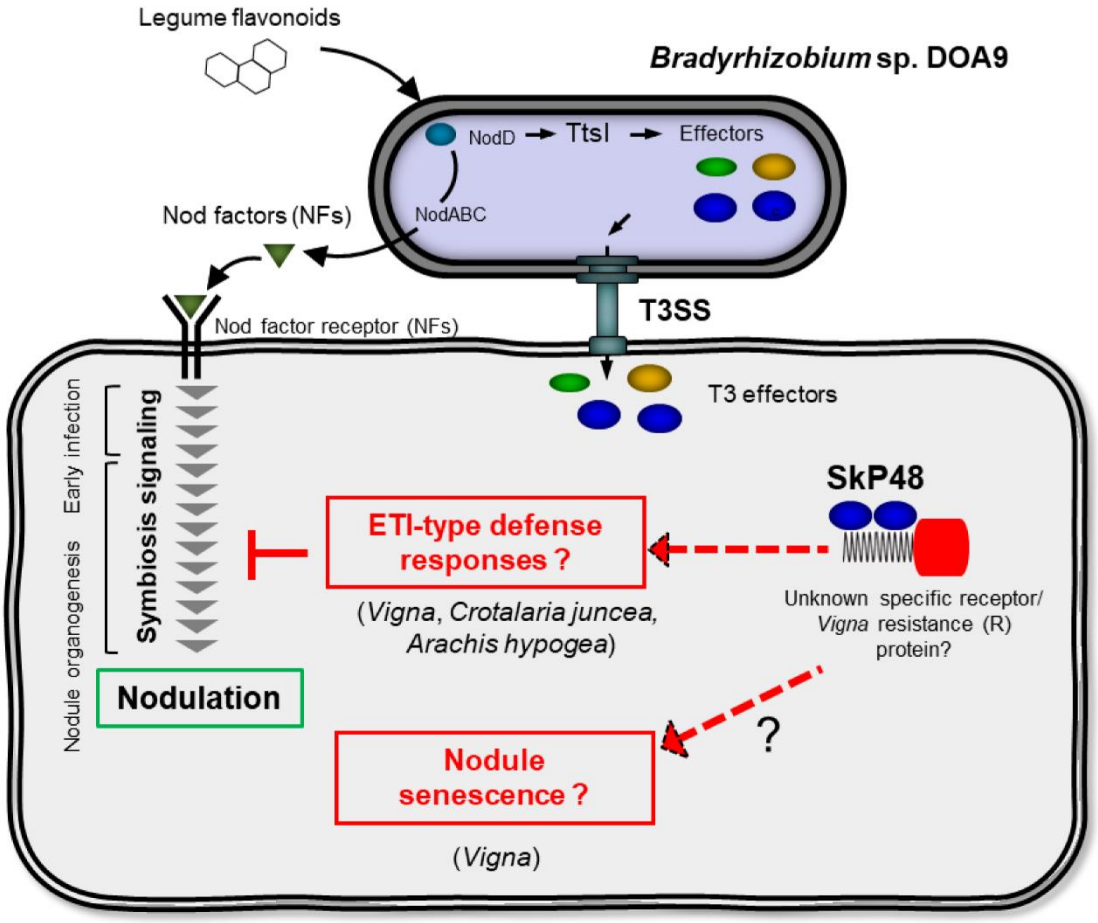

643

644

645 Figure 7

Supplementary Files

This is a list of supplementary files associated with this preprint. Click to download.

- SupplementaryMaterial12921.pdf